Available online at www.sciencedirect.com
SCIENCE DIRECT
Journal of Catalysis 239 (2006) 282–289
JOURNAL OF CATALYSIS
www.elsevier.com/locate/jcat

Preparation of mesostructured barium sulfate and its application in methane activation

Fengbo Li, Guoqing Yuan *

Laboratory of New Materials, Institute of Chemistry, Chinese Academy of Sciences, 100080, Beijing, China

Received 18 October 2005; revised 23 January 2006; accepted 24 January 2006

Available online 6 March 2006

Abstract

Barium sulfate with lamellar and tubular microstructure was developed through a surfactant templating route under different synthesis conditions. Lamellar barium sulfate was synthesized through direct combination of Ba^{2+} and SO_4^{2-} in an aqueous solution containing sodium dodecyl benzene sulfonate (SDBS). Agglomerate barium sulfate nanotubes were obtained by the reaction of Ba^{2+} and $CaSO_4$ in the SDBS aqueous solution. Preparation of regular single barium sulfate nanotubes was achieved by the controlled hydrolysis of dimethyl sulfate in an aqueous solution containing Ba^{2+} and SDBS. As revealed by transmission electron microscopy characterization, the tube wall thickness was 7–8 nm, and the inner diameter was about 6 nm. When such mesostructured barium sulfate was loaded with $VOSO_4$ and sulfuric acid (100%), it performed excellently in catalyzing oxidative conversion of methane to methanol using molecular oxygen. The conversion proceeded at a relatively lower temperature (under 250 °C) than over general solid catalysts, and the selectivity to methanol remained high when methane conversion increased to an acceptable level. When the reaction proceeded stably, the one-pass conversion of methane was about 30%, and the selectivity to methanol could reach 50%.

Keywords: Barium sulfate; Surfactant templating; Lamellar; Nanotube; Methane oxidation; Methanol

1. Introduction

The development of mesostructured inorganic materials has been widely considered one of the most promising areas in recent years. These materials have expected applications in many fields, including catalysis, coatings, membranes, and electronics. A vast body of knowledge of synthesis and physical and chemical properties has been accumulated and thoroughly reviewed [1–3]. Mesostructure build-up of a wide variety of inorganic materials, including metal sulfides, nitrides, oxides, phosphates, and polyoxometalates, has been attempted [4–10]. Generally, the self-assembly mechanism of structure-directing agents is used for the evolution of mesophases. The properties of structure-directing agents may have a significant effect on the alignment and patterning of the resultant mesophases. Surfactants are the most commonly used structure-directing agents. Rapid progress in the synthesis of mesostructured materials has demonstrated the possibility of preparing mesostructured sulfates through the surfactant-templating route [11–13]. Such inorganics have two impressive properties that could stimulate extensive exploration of their mesostructure building and related application in catalysis [14]: they are thermally stable and chemically inert in many extreme conditions, and have attractive potential in the organization of mesostructures and the possibility of combining properties of different components in a unique composite material. To the best of our knowledge, there have been no detailed reports on the synthesis of mesostructured sulfates and related applications in catalysis.

In a recent communication [15], we reported the excellent performance of barium sulfate nanotube arrays in supporting sulfates for low-temperature methane activation. In the present work, we present detailed information on the preparation of three types of mesostructured barium sulfate (lamellar, agglomerate nanotube, and single nanotube) under various preparation conditions.

* Corresponding author. Fax: +86 10 6255 9373.
E-mail address: yuangq@iccas.ac.cn (G. Yuan).

0021-9517/$ – see front matter
doi:10.1016/j.jcat.2006.01.029

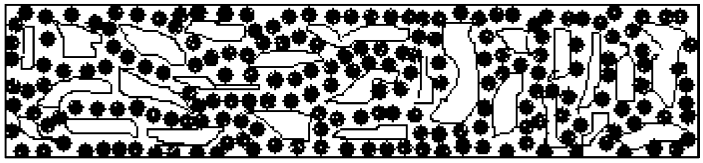

Scheme 1. Schematic illustration of the catalyst particles diluted by fine inert glass beads (100 mesh).

2. Experimental

2.1. Synthesis of mesostructured barium sulfate

The surfactant-templating synthesis was used to develop such mesostructured materials. Anionic surfactant (SDBS) was the organic structure-directing agent. Barium sulfate was generated by three different methods: (1) direct combination of Ba^{2+} and $SO_4{}^{2-}$ in aqueous solution, (2) reaction between $CaSO_4$ and Ba^{2+} in aqueous solution, and (3) controlled hydrolysis of dimethyl sulfate in the presence of Ba^{2+} in aqueous solution.

Lamellar barium sulfate was synthesized through direct combination of Ba^{2+} and $SO_4{}^{2-}$ in aqueous solution containing SDBS. The SDBS (0.025 mol) was dissolved in 150 mL of deionized water in a 500-mL, three-necked, round-bottomed flask containing a magnetic stirring bar and fitted with an additional funnel and condenser. $BaCl_2$ (0.036 mol) dissolved in 50 mL of water was added to the solution dropwise under vigorous stirring. The solution became hazy. After 30 min of stirring, the solution was heated to reflux, then 50 mL of 0.7 M Na_2SO_4 aqueous solution was added dropwise over 90 min under vigorous stirring. After every several drops, the addition was momentarily stopped, to allow the block precipitate to homogenize. After all of the Na_2SO_4 was added, the reaction mixture was kept at reflux for 24 h, cooled to room temperature, and stored for several days. The solution was filtered to collect the solid material. The surfactant molecules in the resulting material were twice extracted by a 50-mL mixture of ethanol and diethyl ether (V/V = 2:1) and a 50-mL mixture of concentrated HCl and ethanol (V/V = 1/5). Finally, hot acetone was used to extract the fresh sample for 3 h or longer, to remove the remaining surfactant molecules.

Agglomerate barium sulfate nanotubes were synthesized by the reaction between Ba^{2+} and $CaSO_4$ in aqueous solution. Then 0.03 mol anhydrous $CaSO_4$, 125 mL of aqueous solution containing SDBS (0.025 mol), and $BaCl_2$ (0.04 mol) were sealed in a 250-mL stainless steel autoclave and heated to 135 °C. The reaction continued for 8 h. The resulting mixture was cooled to room temperature and stored for several days. The solid materials were collected by filtration, and the surfactant molecules were removed as in the preceding method.

Single barium sulfate nanotubes were synthesized by controlled hydrolysis of dimethyl sulfate in aqueous solution containing Ba^{2+} and SDBS. The 0.025 mol SDBS was dissolved in 100 mL of deionized water and placed into a 500-mL three-necked, round-bottomed flask. Then 50 mL of 0.7 M Ba^{2+} aqueous solution was added dropwise. When the solution became hazy, 7 mL of pure dimethyl sulfate was added; the reaction mixture was kept at 80–85 °C under vigorous stirring for 36 h, then cooled to room temperature and stored for several days. The solid material was collected and purified as in the foregoing methods.

2.2. Preparation of the catalyst for methane oxidation and catalytic activity measurement

Well-developed $BaSO_4$ nanotubes were used to support $VOSO_4$ and concentrated sulfuric acid for oxidation of methane to methanol. $VOSO_4$ was introduced by impregnating the fresh nanotubes in $VOSO_4$ aqueous solution, followed by drying in vacuum at room temperature. Before the catalyst test, the fresh sample was doped with concentrated sulfuric acid (100–103%), which was prepared by bubbling SO_3 into 98% H_2SO_4. In this case, the solubility of sulfate in concentrated sulfuric acid could be neglected because the amount of sulfuric acid used was just sufficient to dope the solid catalyst. Methane oxidation was conducted in a conventional fixed-bed reactor. The acidified sample was mixed with glass beads (100 mesh) of the same volume and packed in a conventional fixed bed reactor (Ti alloy, Φ 0.8 cm × 30 cm). The catalyst particles were diluted by fine inert glass beads, as shown schematically in Scheme 1. The dead volume was filled with glass wool. Argon was used as a carrier gas. Argon, oxygen, and methane flows were controlled by mass flow control. The reactor column was heated in an electronic tube furnace with three independent heating units (1 cm × 10 cm) controlled by temperature-program controllers (sensitivity ±0.5 °C). The product analysis was performed on a DB5 column (30 m × 0.25 mm) using a VG Trio200 with a thermal conductivity detector (TCD) or mass spectrometry (MS) detector. He was used as the carrier gas. The column temperature increased from 60 to 300 °C at a rate of 10 °C/min and maintained at 60 °C for 2 min. The working temperature of the TCD was 180 °C, and the ion source temperature of the MS detector was 200 °C. Conversion and selectivity are defined as

$$\%\text{conversion} \equiv \frac{[CH_4]_{\text{inlet}} - [CH_4]_{\text{outlet}}}{[CH_4]_{\text{inlet}}} \times 100$$

and

$$\%\text{selectivity to methanol} \equiv \frac{[CH_3OH]}{[CH_4]_{\text{inlet}} - [CH_4]_{\text{outlet}}} \times 100.$$

2.3. Characterization of the as-synthesized materials

X-ray photoelectron spectroscopy (XPS) was used to determined the surface atomic ratio of V(IV) to Ba^{2+}. The XPS measurement was carried on an ESCALab200I-XL (VG Science) spectrometer using Al-K_α X-radiation at 15 kV × 20 mA, equipped with a hemispherical electron analyzer. All XPS peak

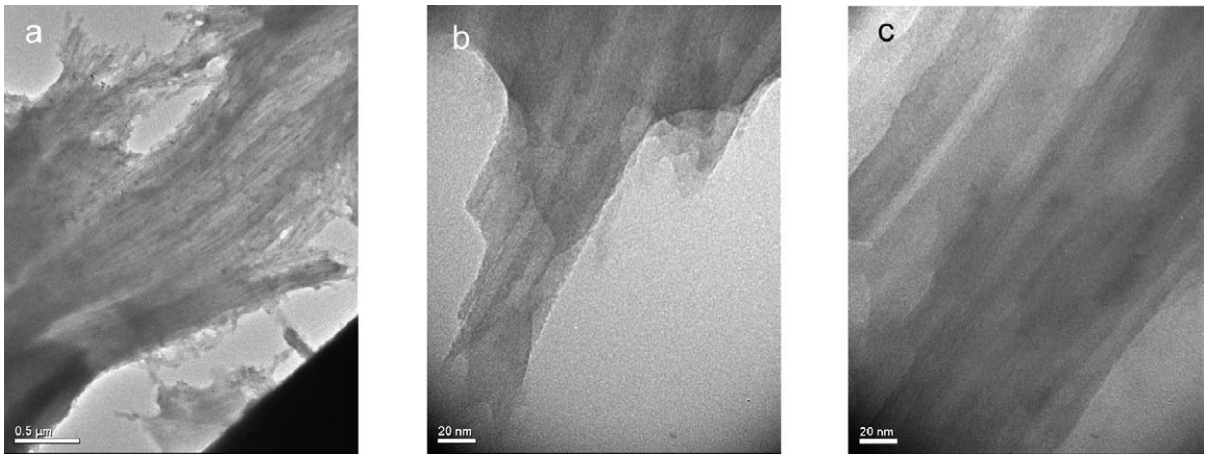

Fig. 1. Lamellar barium sulfates synthesized through direct combination of Ba^{2+} and SO_4^{2-} in SDBS aqueous solution. (a) Depicts the lamellar architectures with lower magnification and (b) and (c) present closer views of the lamellar structures.

positions were calibrated by the binding energy of C_{1s} at 284.6 eV as reference. Eclipse V2.1 data analysis software supplied by the manufacturer was used for manipulation of the acquired spectra. The XPS intensity ratio of the signals from the metal elements of the sulfates and the support (I_M^{n+}/I_{Ba}^{2+}) reflects the dispersion of the sulfates over the support. Good dispersion leads to a high intensity ratio (I_M^{n+}/I_{Ba}^{2+}). The final value was in the range of 0.1–0.16. Transmission electron microscopy (TEM) is the main characterization tool in this work. It gives clear images of microstructures of the as-synthesized sample and reliable information about the nanoarchitecture building under various preparation conditions. Porosity properties of the regular barium sulfate nanotubes are characterized by N_2 adsorption analysis conducted on a Quantachrome Autosorb Automated Gas Sorption System.

3. Results and discussion

3.1. Preparation of mesostructured barium sulfate

Lamellar barium sulfates were obtained by rapid precipitation of barium sulfate through the direct combination of Ba^{2+} and SO_4^{2-} in SDBS aqueous solution. Fig. 1 shows the lamellar microstructures of the as-synthesized sample. Fig. 1a depicts the lamellar architectures with lower magnification, and Figs. 1b and 1c present closer views of the lamellar structures. From these TEM images, different layers of the given local region could be distinguished; the gaps between layers are uniform. However, such micro architectures are in a very low-order state, and when the surfactant molecules are removed, the remaining solid structures are unstable. In aqueous solution, if surfactant molecules (SDBS) direct the buildup of mesophases, then spherical or cylindrical micelles, or even higher-order phases, may be formed through self-assembly [16]. In this case, rapid precipitation of barium sulfate from the aqueous solution makes the structure-directing agents (SDBS) ineffective. The assembly of SDBS anions over the fresh barium sulfate precipitate and the subsequent gradual fusion of such little chips lead to the final lamellar microstructures.

Tubular barium sulfate is obtained through the self-assembly mechanism of SDBS. There are two sources of barium sulfate: reaction between $CaSO_4$ and Ba^{2+} in aqueous solution and controlled hydrolysis of dimethyl sulfate in the presence of Ba^{2+}. In aqueous solution, there is a marked difference between the solubility product constants of $CaSO_4$ and $BaSO_4$. $BaSO_4$ is less soluble in water than $CaSO_4$ (K_{BaSO_4}/K_{CaSO_4} is about 0.44×10^{-5} at 25 °C). In the presence of Ba^{2+}, the dissolution equilibrium of $CaSO_4$ in aqueous solution is broken. The sulfates are precipitated with Ba^{2+} to form more insoluble $BaSO_4$ and $CaSO_4$ dissolved continuously to maintain the dissolution equilibrium. The TEM images of the as-synthesized sample are shown in Fig. 2. Visually, such microarchitectures could be considered agglomerate nanotubes. Significantly, it can be established here that controlling the precipitation rate and model of barium sulfate can facilitate the generation of high-order microarchitectures. Controlled precipitation of barium sulfate through reaction between Ba^{2+} and $CaSO_4$ is not a very efficient process for controlling generation of barium sulfate, but it improves the regularity of the final microarchitecture, based on a comparison of Figs. 1 and 2.

Synthesis of regular barium sulfate nanotubes (BSNT) was achieved by SDBS templating hydrolysis of dimethyl sulfate in the presence of Ba^{2+} in aqueous solution. Fig. 3 shows TEM images of such well-prepared single barium sulfate nanotubes. Fig. 3a shows a single barium nanotube and Fig. 3b is the TEM image of several folded nanotubes. It is demonstrated that the resulting microstructure is well organized as cubic tubular structures with a hollow center. The outer diameter is about 20 nm, the tube wall thickness is 7–8 nm, and the inner diameter is about 4–7 nm. Nitrogen sorption analyses were carried out to characterize the porosity properties. The isotherm of the resultant materials is very similar to a type IV isotherm. There is a steep slope at high relative partial pressure and a hysteresis loop (Fig. 4). The isotherm and adsorption–desorption curve are typical for mesoporous materials. A BET surface area of about 42 m^2/g was calculated for the resultant materials. The pore size distribution curve obtained by the DH method shows that the pore size is mainly in the range of

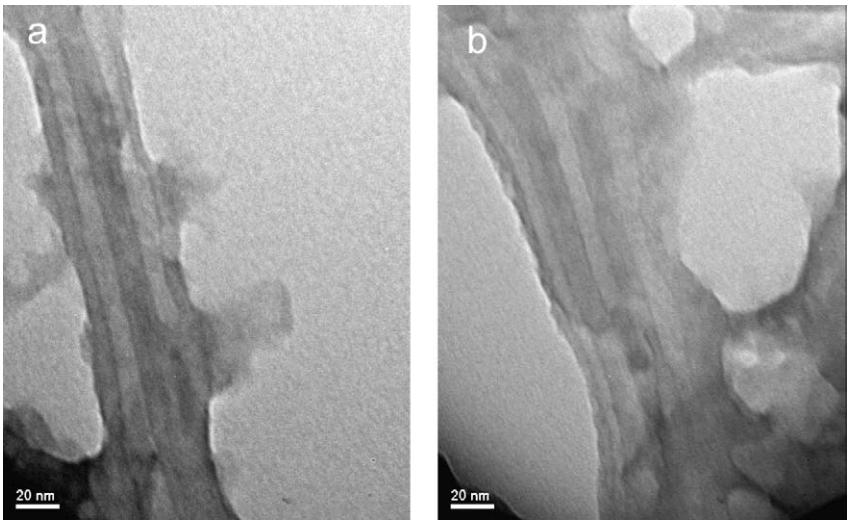

Fig. 2. Tubular barium sulfate obtained through the reaction between $CaSO_4$ and Ba^{2+} in SDBS aqueous solution.

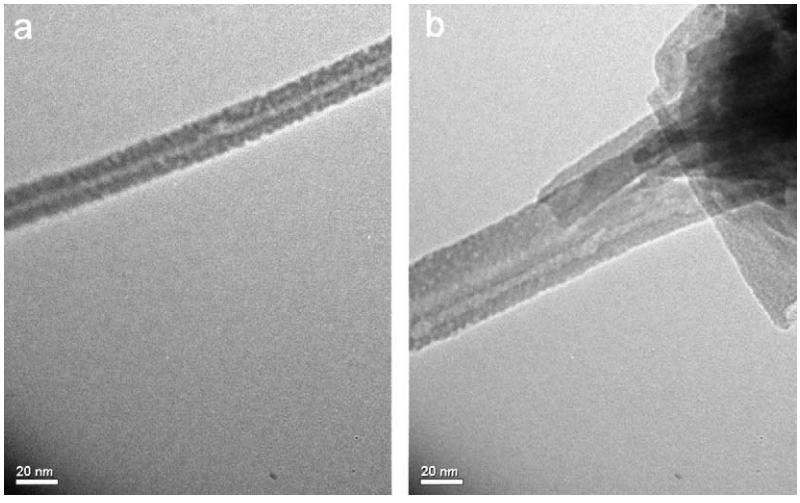

Fig. 3. TEM images of such well-prepared barium sulfate nanotubes. (a) Shows a single barium nanotube and (b) is the image of several folded nanotubes.

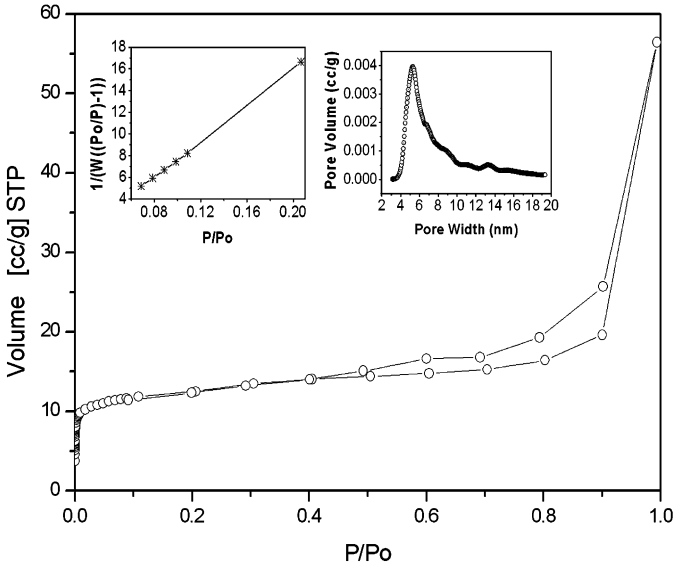

Fig. 4. N_2 adsorption isotherm at −195.65 °C and BET plot (the left insert) and pore size distribution (the right insert) for barium sulfate nanotubes.

4–7 nm, confirming the information on nanotube size obtained from the TEM images. The total pore volume is 0.087 cc/g ($P/P_0 = 0.99378$). The lamellar and agglomerate tubular barium sulfates have very low surface areas (lamellar, 2.3 m^2/g; agglomerate tubular, 6.7 m^2/g) and poor porosity properties.

The growth mechanism of barium sulfate nanotubes may involve two main steps: the generation of barium sulfate and the organization of the nanostructure directed by the surfactant templates. In our experimental observation, the resulting nanostructure of the as-synthesized materials has a subtle relationship to the hydrolysis of dimethyl sulfate, which leads directly to the generation of barium sulfate. A schematic illustration of the possible hydrolysis process of dimethyl sulfate is shown in Fig. 5. Because dimethyl sulfate is not soluble in aqueous solution, the hydrolysis may occur at the interface between the two phases. SDBS, which had been added to the $BaCl_2$ aqueous solution before dimethyl sulfate, could facilitate the high dispersion of dimethyl sulfate. As a result, it may self-assemble to form a membrane over the interface between the dimethyl sulfate phase and the aqueous phase, and

dimethyl sulfate molecules can diffuse across it. Dimethyl sulfate molecules in the aqueous phase are hydrolyzed to release sulfate, after which barium sulfate is generated and precipitated on the hydrophilic side of the surfactant membrane. The hydrolysis of dimethyl sulfate depicted above can be understood as a controlled sulfate-release process, which may be the rate-determining step for the generation of barium sulfate. Fig. 6 shows the TEM images of tubular structures built at the incipient state of mesophase patterning from a sample obtained in a highly dilute barium chloride aqueous solution. As proposed above, barium sulfate was generated and precipitated on the hydrophilic side of the column formed by the self-assembly of surfactant molecules. Such a mechanism governs the organization of tubular barium sulfate nanostructures.

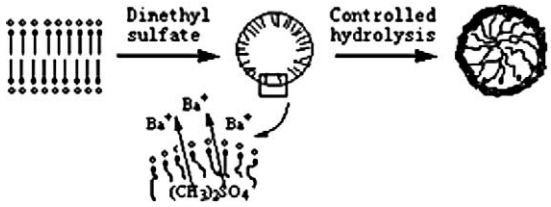

Fig. 5. Schematic illustration of the growth of barium sulfate nanotubes.

Many factors affect the resulting nanostructure, including surfactant concentration, surfactant chain length, synthesis temperature, barium sulfate source, and postsynthesis treatment. The effects of the barium sulfate source have been discussed in the foregoing paragraphs. Another important parameter is the postsynthesis treatment—surfactant removal. In our experiments, the surfactant molecules in the resultant composite solid were removed though a liquid solvent extraction method. Compared with calcination, this is a milder process and may minimize structural damage. Fig. 7 shows TEM images of the sample derived from the same precursors as shown in Fig. 3, but with the surfactant molecules removed by calcination at 450 °C for 6 h in air, not by liquid solvent extraction. Single barium nanotubes can also be obtained (Fig. 7a) under such calcination in air, but structural damage is very significant. As revealed in Fig. 7b, there is a strong possibility that large-scale

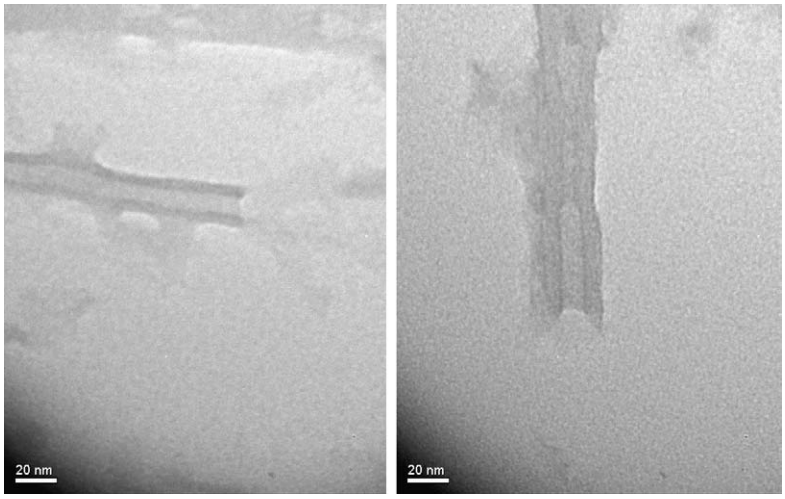

Fig. 6. TEM images of tubular structures formed in the incipient state of mesophase patterning.

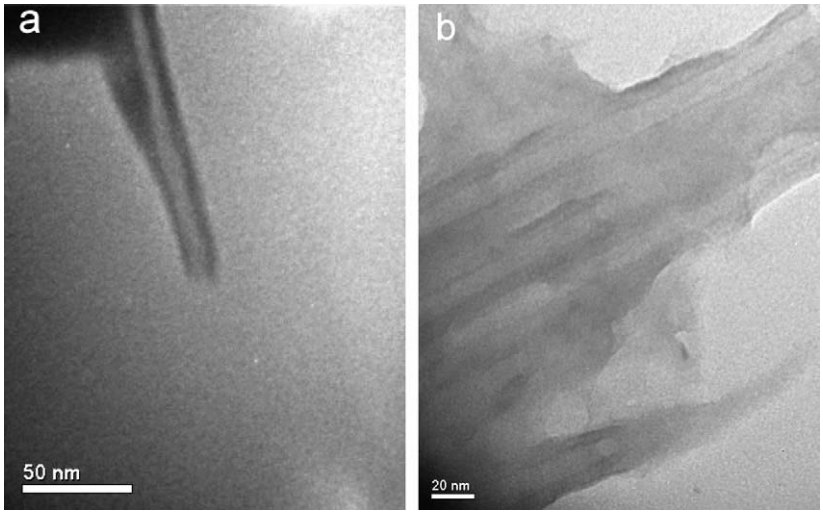

Fig. 7. TEM images of the sample derived from the same precursors as shown in Fig. 3, but the surfactant molecules were removed by calcination at 450 °C for 6 h in air.

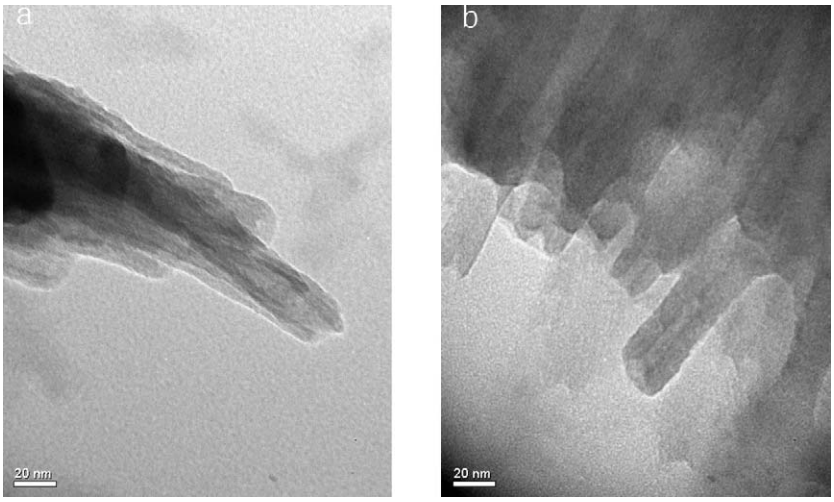

Fig. 8. (a) Is the TEM image of barium sulfate nanotubes impregnated with $VOSO_4$; (b) is the TEM image of the used catalyst.

microstructure collapse of the sample occurs during the calcination process.

3.2. Oxidation of methane to methanol

As discussed above, barium sulfate has great potential in catalysis applications because of two impressive properties. Here, well-defined BSNTs were used to support $VOSO_4$ and concentrated sulfuric acid for the low-temperature oxidation of methane to methanol. Compared with BSNTs, lamellar and agglomerate tubular barium sulfate have very low surface areas and poor thermal stability and thus are not suitable catalyst supports. The fresh BSNTs were impregnated in $VOSO_4$ aqueous solution, followed by drying in vacuum at room temperature. Fig. 8a shows the dispersion state of the introduced $VOSO_4$. The BSNTs in the array are all loaded with $VOSO_4$. The newly impregnated $VOSO_4$ layer can be visually distinguished from the original tube wall of the BSNTs. Before the catalytic activity test, a minimum amount of concentrated sulfuric acid was used to dope the catalyst sample.

Table 1 lists the results of the catalytic activity test. Control experiments were conducted over $VOSO_4/BaSO_4$, blank $BaSO_4$ nanotubes, and acidified $BaSO_4$ nanotubes under the same reaction conditions as acidified $VOSO_4/BaSO_4$. Blank $BaSO_4$ nanotubes showed no activity for the oxidation of methane. $VOSO_4/BaSO_4$ and acidified $BaSO_4$ had minimal methane conversion. The main oxidation products are CO_2 and CO for $VOSO_4/BaSO_4$, and methanol and formaldehyde for acidified $BaSO_4$. Acidified $VOSO_4/BaSO_4$ showed relatively high one-pass methane conversion (about 30%). Increasing reaction temperature brought a marked increase in methane conversion, whereas the selectivity to methanol fluctuated in a narrow range of 50–60%, with no sharp decrease observed. Methanol and formaldehyde are the intermediate products of methane oxidation from methane to carbon dioxide when oxygen molecules are used as an oxidant over solid-state catalysts. The selectivity of intermediate products of any consecutive reaction always increases markedly with decreasing conversion [17–22]. But in our experimental observation, the selectivity to methanol slightly increased with increasing methane conversion due to reaction temperature elevation. There is a strong possibility that methanol has evolved through a different mechanism than the partial oxidation over general solid catalysts using dioxygen. A mechanistic issue arising here is the role of concentrated sulfuric acid doping.

Before discussing this issue, we first need to elucidate how the experimental data were obtained from the FBR test. In the

Table 1
Experimental results of catalytic methane oxidation activity measurement

Catalysts	Reaction temperature (°C)	CH_4 conversion[a] (%)	Selectivity[a] (%)				Carbon balance[b] (%)
			CH_3OH	CH_2O	CO	CO_2	
$BaSO_4$	220	0	0	0	0	0	100
$VOSO_4/BaSO_4$	220	1.8	1.7	2.3	17.9	79.1	100
$H_2SO_4/BaSO_4$	220	2.6	59	10.7	14	14.3	100
$H_2SO_4/VOSO_4/BaSO_4$	220	30.9	57.5	5.6	13.6	19.9	98.9
$H_2SO_4/VOSO_4/BaSO_4$	200	27	57	5.2	14.3	20.5	99.1
$H_2SO_4/VOSO_4/BaSO_4$	180	16	52	8.8	15.2	21	99.5

Note. Reaction conditions: 5 g catalysts were mixed with glass beads (100 mesh) of the same volume and packed in a conventional fixed bed reactor. The test was carried out under atmosphere pressure. Argon was used carrier gas ($P_{CH_4}/P_{O_2} = 2.0$, $P_{CH_4} = 20$ kPa, flow rate = 20 mL/min).

[a] The reported catalytic activity data were determined after 80 min on the stream. The activity fluctuated markedly in the first 80 min. In the following test periods from 80 to 200 min, the activity fluctuation was negligible.

[b] The level of carbon balance is defined as $([\text{carbon containing molecules}]_{outlet}/[CH_4]_{inlet}) \times 100$.

catalyst column, the catalyst particles were diluted by fine inert glass beads (100 mesh) (Scheme 1) to decouple the hydrodynamics and kinetics of the reactor. The fine dilution particles determine the hydrodynamic performance, and the catalyst particles dictate the kinetic behavior. This bed dilution was also applied here to obtain a sufficient bed length, which can increase the contact time between the reactant flow and the catalyst particles, thereby reducing the space velocity [23]. In many previous studies on partial methane oxidation over solid catalysts at high temperature [22], high space velocity was applied to increase the selectivity to methanol; however, high space velocity and short contact time led to very low methane conversion. In this work, high methane conversion was achieved by maintaining the space velocity at a low and acceptable level, but the selectivity to methanol was >50%. This novelty may be due mainly to concentrated sulfuric acid doped over the sulfate surface. As shown in Table 1, the test results without H_2SO_4 doping were very poor. $BaSO_4$ and $VOSO_4$ are soluble in hot concentrated sulfuric acid. Under methane oxidation temperature, the doped H_2SO_4 can dissolve the surface sulfate species, and H_2SO_4 films containing $BaSO_4$ and $VOSO_4$ are formed. Fig. 8b shows a TEM image of the catalyst after the activity test. Compared with Fig. 8a, here the solution of $BaSO_4$ and $VOSO_4$ causes fusion of the tubular structures. The H_2SO_4 films are the active sites for methane partial oxidation.

From a certain angle, methane oxidation over acidified $VOSO_4/BaSO_4$ can be considered a heterogenized version of the experiments in liquid sulfuric acid. Many high-yield systems for the conversion of methane to methyl derivatives have been operated in liquid sulfuric acid at low temperature [24–35]. Under strong acidic conditions, VO^{2+} can be converted to the more powerful oxidizing agent VO_2^+ by dioxygen [$E^0 = 1.0$ V VO_2^+/VO^{2+}; $E^0 = 0.337$ V VO^{2+}/V^{3+}; $E^0 = 0.17$ V SO_4^{2-}/H_2SO_3; $E^0 = 1.22$ V $O_2(g)/H_2O$]. In sulfuric acid containing VO_2^+, methane can be oxidized to form methyl bisulfate, which has antioxidant properties [26]. This compound can be readily hydrolyzed to methanol; the catalytic cycle is shown in Scheme 2. For homogeneous systems, it is difficult to separate the products from strong acid media. But in this heterogenized process, methanol can be readily separated from the thin H_2SO_4 films through mass transfer process between the bulk flow and the solid catalyst surface. This indirect methane oxidation via antioxidative methyl bisulfate at low temperature makes the conversion process show higher selectivity to methanol than other processes over solid catalysts at high temperature (above 500 °C). As shown in the catalytic cycle, methanol is the final product; thus, methane conversion can increase without reducing methanol selectivity. The low reaction temperature could reduce the possibility of further methanol oxidation. This also increases the apparent selectivity to methanol. Barium sulfate dissolved in H_2SO_4 film is another promoting factor for methane oxidation. Barium sulfate doped with H_2SO_4 showed 2.6% methane conversion and 59% selectivity to methanol. Recent studies [27,36] showed that the cations of Group IIA can catalyze functionalization of methane in liquid sulfuric acid solution. Here Ba^{2+} in the H_2SO_4 film

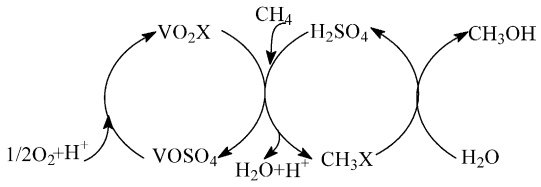

Scheme 2. Proposed methanol formation catalytic cycles. X = OSO_3H.

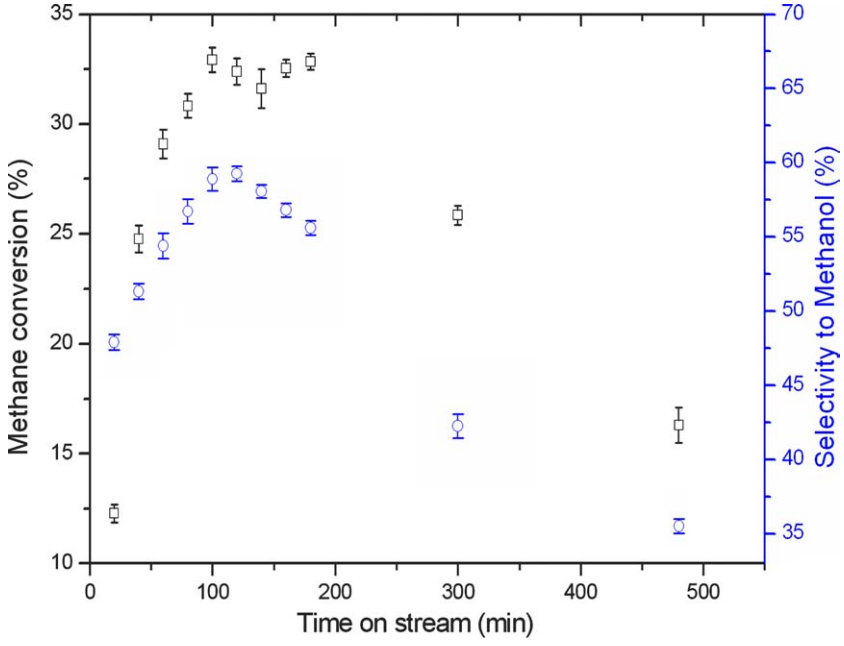

Fig. 9. The time-on-stream data of acidified $VOSO_4/BaSO_4$. Reaction conditions: 5 g catalysts were mixed with glass beads (100 mesh) of the same volume and packed in a conventional fixed bed reactor. The test was carried out under atmosphere pressure. Argon was used carrier gas ($P_{CH_4}/P_{O_2} = 2.0$, $P_{CH_4} = 20$ kPa, flow rate = 20 mL/min). (□) The methane conversion and (○) the selectivity to methanol.

shows some promoting effect on the oxidative methane conversion.

Fig. 9 shows time-on-stream data for acidified $VOSO_4$/$BaSO_4$. Its activity fluctuated markedly in the first 60 min. In the subsequent test periods from 80 to 200 min, the activity fluctuation was negligible, and the one-pass conversion of methane was around 30%. The selectivity to methanol from 80 to 200 min was mainly in the range of 50–60%. After the reaction ran for 300 min, the catalyst showed a propensity to deactivation. At 480 min, the one-pass methane conversion decreased to about 16%, and the selectivity to methanol decreased to about 35%. This propensity toward deactivation may be due to two physicochemical processes: (1) the gradual fusion of tubular structures resulting from the dissolution of sulfates in hot H_2SO_4 films, and (2) the redispersion of H_2SO_4 in the reactor column, that is, the gradual wetting of inert glass beads. The gradual fusion of tubular structures during the activity testing, which has been clearly demonstrated by the TEM images of the used catalyst (Fig. 8b), could lead to gradual loss of catalytic surface area and cause catalyst deactivation. With the mass transfer in the catalyst column, the doped H_2SO_4 could be transported to coat the inert glass beads used as the bed dilution agents. This would cause the loss of the surface active sites that are the hot H_2SO_4 films containing $VOSO_4$ and $BaSO_4$.

4. Conclusion

This work studied three synthesis routes for developing mesostructured barium sulfate. The three routes used three different sources of barium sulfate, but all used SDBS as the structure-directing agent. When barium sulfate was precipitated by direct combination of Ba^{2+} and sulfate in aqueous solution, lamellar structures were developed. When barium sulfate was generated by the reaction between $CaSO_4$ and Ba^{2+} in aqueous solution, the resultant materials showed a certain amount of regularity in mesostructure organization. BSNTs were finally obtained through controlled hydrolysis of dimethyl sulfate in the presence of Ba^{2+} in aqueous solution. The resultant barium nanotubes have a regular tubular structure, with a tube wall thickness of 7–8 nm and an inner diameter of about 6 nm. Such well-prepared mesostructured barium sulfate has great potential for applications in catalysis. It performed excellently in supporting $VOSO_4$ and concentrated sulfuric acid for low-temperature oxidation conversion of methane to methanol. The one-pass conversion of methane was about 30%, and the selectivity to methanol could reach 50% when the reaction was stable.

Such a heterogenized version of activating methane under strong acidic conditions has many advantages over common solid catalysts for methane oxidation. The conversion proceeds at relatively lower temperatures (under 250 °C), and a high selectivity to methanol can be maintained when methane conversion increases to practicable levels. Although numerous related issues require further investigation, such a methane activation process provides useful information in the development of a direct methane-to-methanol process on a large scale.

References

[1] P.M. Ajayan, Chem. Rev. 99 (1999) 1787.
[2] C. Scanchez, G.J.A.A. Soler-Illia, F. Ribot, T. Lalot, C.R. Mayer, V. Cabuil, Chem. Mater. 13 (2001) 3061.
[3] K.J.C. Bommel, A. Friggeri, S. Shinkai, Angew. Chem. Int. Ed. 42 (2003) 980.
[4] R. Tenne, L. Margulis, M. Genut, G. Hodes, Nature 360 (1992) 44.
[5] Y. Feldman, E. Wasserman, D.J. Srolovitz, R. Tenne, Science 267 (1995) 222.
[6] E.J.M. Hamilton, S.E. Dolan, C.E. Mann, H.O. Colijin, C.A. McDonald, S.G. Shore, Science 260 (1993) 659.
[7] W. Tremel, Angew. Chem. Int. Ed. 38 (1999) 2175.
[8] G.R. Patzke, F. Krumeich, R. Nesper, Angew. Chem. Int. Ed. 41 (2002) 2446.
[9] G. Wu, L. Zhang, B. Cheng, T. Xie, X. Yuan, J. Am. Chem. Soc. 126 (2004) 5976.
[10] T. Yamase, M.T. Pope (Eds.), Polyoxometalate Chemistry for Nano-Composite Design, Kluwer Academic, New York, 2002.
[11] P.T. Tanev, T.J. Pinnavaia, Science 267 (1995) 865.
[12] Q.S. Huo, D.I. Margolese, U. Ciesla, P.Y. Feng, T.E. Gler, P. Sieger, R. Leon, P.M. Petroff, F. Schuth, G.D. Stucky, Nature 368 (1994) 317.
[13] D.Y. Zhao, J.L. Feng, Q.S. Huo, N. Melosh, G.H. Fredrichson, B.F. Chmelka, G.D. Stucky, Science 279 (1998) 548.
[14] M. Tiemann, M. Froba, Chem. Mater. 13 (2001) 3211.
[15] F. Li, G. Yuan, Chem. Commun. 17 (2005) 2238.
[16] J.H. Fendler, E.J. Fendler, Catalysis in Micellar and Macromolecullar System, Academic Press, New York, 1975.
[17] H.D. Gesser, N.R. Hunter, C.B. Prakash, Chem. Rev. 85 (1985) 235.
[18] F. Arena, A. Parmaliana, Acc. Chem. Res. 36 (2003) 867.
[19] K. Otsuka, M. Hatano, J. Catal. 108 (1987) 252.
[20] D. Spencer, J. Catal. 109 (1988) 187.
[21] T. Weng, E.E. Wolf, Appl. Catal. A 96 (1993) 383.
[22] Y. Wang, K. Otsuka, J. Catal. 155 (1995) 256.
[23] S.T. Sie, Rev. Inst. Franc. Pétrol. 46 (1991) 501.
[24] D. Wolf, Angew. Chem. Int. Ed. 37 (1998) 3351.
[25] X. Gang, H. Birch, Y. Zhu, H.A. Hjuler, N.J. Bjerrum, J. Catal. 196 (2000) 287.
[26] N. Basiches, T.E. Hogan, A. Sen, J. Am. Chem. Soc. 118 (1996) 13111.
[27] S. Mukhopadhyay, A.T. Bell, J. Am. Chem. Soc. 125 (2003) 4406.
[28] S. Mukhopadhyay, M. Zerella, A.T. Bell, V. Srinivas, Chem. Commun. 4 (2004) 472.
[29] R.A. Periana, D.J. Taube, S. Gamble, H. Taube, T. Satoh, H. Fuji, Science 280 (1998) 560.
[30] R.A. Periana, O. Mirinov, D.J. Taube, S. Gamble, Chem. Commun. 20 (2002) 2376.
[31] S. Mukhopadhyay, A.T. Bell, Adv. Synth. Catal. 346 (2004) 913.
[32] M. Zerella, S. Mukhopadhyay, A.T. Bell, Org. Lett. 5 (2003) 3193.
[33] Y. Taniguchi, T. Hayashida, H. Shibasaki, D. Piao, T. Kitamura, T. Yamaji, Y. Fujiwara, Org. Lett. 1 (1999) 557.
[34] R.A. Periana, O. Mirinov, D. Taube, G. Bhalla, C.J. Jones, Science 301 (2003) 814.
[35] I.V. Kozhevnikov, in: E.G. Derouane (Ed.), Catalytic Activation and Functionalisation of Light Alkanes, Kluwer Academic, Dordrecht, 1998, p. 75.
[36] M. Asaddullah, T. Kitamura, Y. Fujiwara, Angew. Chem. Int. Ed. 39 (2000) 2475.